Role of plasmon decay in secondary electron emission in the nearly-free-electron metals. Application to aluminum*

M. S. Chung and T. E. Everhart
Department of Electrical Engineering and Computer Sciences, and the Electronics Research Laboratory, University of California, Berkeley, California 94720
(Received 5 January 1976)

In this paper, a theoretical analysis of secondary electron emission in the nearly-free-electron (NFE) metals is presented. Restricting ourselves to excitation of secondary electrons (SE's) from the valence (or conduction) band only, we investigate the roles played by screened electron-electron scattering and by volume- and surface-plasmon decay in the excitation of SE's. Using the complex dielectric constant in the random-phase approximation we demonstrate that an important source of low-energy SE's may arise from the decay of long-wavelength surface and volume plasmons via near vertical interband transitions. A simple transport theory based on the work of Berglund and Spicer is developed to treat the SE escape problem approximately assuming an idealized model of the solid-vacuum surface barrier. Model calculations of the external SE energy distribution curve (EDC) and its derivative are presented for aluminum. The results are in reasonable agreement with some recent experimental EDC's obtained by a number of authors on clean Al samples. We tentatively conclude that an appreciable contribution to the total number of low-energy SE's emitted from NFE metals under kilovolt electron bombardment may come from the decay of surface and volume plasmons into single-electron excitations.

I. INTRODUCTION

The phenomenon of secondary electron emission (SEE) in solids has received considerable attention in the past.[1–13] In virtually all theoretical treatments of SEE in solids, secondary electrons (or SE's as they are commonly denoted) are assumed to be generated through direct electron-electron scattering between the incident (or primary) eletrons and the electrons associated with atoms in the solid. An SE excitation function derived by Streitwolf[4] utilizing an unscreened Coulomb potential has been used most often.

It is well known[14,15] that owing to the dynamic screening of the pure Coulomb potential, the conduction or valence electrons in many solids can take part in collective oscillations known as plasma oscillations or plasmons. A large number of characteristic energy-loss experiments (using electrons in the keV range) have demonstrated the existence of both volume and surface plasmons in many solids. An extensive list of references on characteristic energy-loss experiments can be found in Refs. 16 and 17. Theoretically, it has been shown[14] that plasmons should constitute a very important energy-loss mechanism for incident fast electrons in many solids. This has been confirmed by experiments.[16,17]

In an actual solid, a volume plasmon once excited can decay via the mechanism of interband transitions. Pines[18] and Ferrell[19] have given theoretical expressions governing the rate of this decay process. Plasmon decay via interband transitions can occur even for plasmons of very long wavelengths, the transitions in this case being nearly vertical in the reduced-zone scheme. [In a free-electron gas, volume plasmons cannot decay into a *single* electron-hole pair unless their wave vectors exceed a critical value if one restricts oneself within the random-phase approximation (RPA).[14]] Because of the possibility of plasmon decay via interband transitions, it is conceivable that electron emission can result from the decay of plasmons created by external radiation. Steinmann and Skibowski[20] have attributed observed peaks at the plasma frequency in the photoyield spectra of aluminum films to the decay of plasmons via interband transitions. With respect to SEE, Gornyi[21] appears to have been the first to point out that plasmon decay into single electron excitations probably plays a role in SEE in some solids. Very weak structures in the experimentally measured SE energy distribution curves (EDC's) from aluminum were attributed by him to plasmon decay.[22] The observed structures occured at SE kinetic energies in vacuum equal to $\hbar\omega - \phi$, where $\hbar\omega$ is the surface- or volume-plasmon energy and ϕ is the work function.

Subsequently, various authors have reported the observation of similar structures in the SE EDC's of Al.[23–26] Some of these authors[25,26] have also attributed the origin of the observed structures to plasmon decay. However, to the best of our knowledge, no one has yet given a quantitative theoretical analysis of the possible role played by plasmon decay in SEE.

In this paper, we present a detailed quantitative analysis of SEE in the nearly-free-electron (NFE)

metals, restricting ourselves to excitation of SE's from the valence (or conduction) band only. The roles played by screened electron-electron scattering as well as volume- and surface-plasmon decay are considered. The results of actual model calculations of the SE EDC are presented for aluminum and compared with existing experimental data. The random-phase approximation is used throughout our analysis.

II. SE EXCITATION: VOLUME-PLASMON DECAY

In this section, we analyze the excitation of SE's in solids by the decay of volume plasmons generated by the incident fast electrons. We describe the crystal electrons by the Bloch scheme, in which the one-electron states are described by a band index l and reduced wave vector $\vec{k}$. We are interested in the process in which an incident fast electron of initial momentum $\hbar\vec{K}_0$ and energy E_0 interacts with a crystal electron in an initial state $|l,\vec{k}\rangle$, causing it to undergo a transition to a new state $|l',\vec{k}'\rangle$. After the interaction, the incident electron has a final momentum $\hbar\vec{K}_1$. Both the initial and final states of the incident primary electron are assumed to be describable by plane waves. Applying the Fermi golden rule to the scattering act and using the RPA, we can write the transition probability per unit time for the process just described as

$$W(l,\vec{k}\to l'\vec{k}') = \frac{32\pi^3 e^4}{\hbar\Delta^2 q^4}\,\frac{|(l'\vec{k}'|l\vec{k})|^2}{|\epsilon(\vec{q},\omega)|^2} \times \delta_{\vec{k}',\vec{k}+\vec{q}}\,\delta(E_{l\vec{k}'} - E_{l\vec{k}} - \hbar\omega), \tag{1}$$

where $\vec{q}=\vec{K}_0-\vec{K}_1$, and

$$(l'\vec{k}'|l\vec{k}) = \frac{1}{\Delta_0}\int_0 u^*_{l'\vec{k}'}(\vec{r})u_{l\vec{k}}(\vec{r})\,d\vec{r}. \tag{2}$$

In (1), Δ is the volume of the solid, $E_{l'\vec{k}'}$ and $E_{l\vec{k}}$ are the one electron energy eigenvalues of the two Bloch orbitals taking part in the transition, and $\epsilon(\vec{q},\omega)=\epsilon_1(\vec{q},\omega)+i\epsilon_2(\vec{q},\omega)$ is the RPA longitudinal dielectric constant for Bloch electrons.[14,27] Also, $\hbar\omega$ is the energy loss suffered by the incident electron, i.e., $\hbar\omega=\hbar^2K_0^2/2m-\hbar^2K_1^2/2m=E_0-E_1$. In (2), $u_{l\vec{k}}$ and $u_{l'\vec{k}'}$ are the periodic part of the Bloch functions, so that $\langle\vec{r}|l\vec{k}\rangle=\Delta^{-1/2}\times e^{i\vec{k}\cdot\vec{r}}u_{l\vec{k}}(\vec{r})$. Δ_0 is the unit-cell volume and $\int_0$ implies integration over a unit-cell volume.

Equation (1) is a straightforward generalization of an expression given by Ritchie[28] (for a free-electron gas) to the case of Bloch electrons. In (1) local field corrections to the dielectric constant are ignored. A concise derivation of (1) is outlined in Appendix A.

The allowed transitions in (1) can be either intraband ($l'=l$) or interband ($l'\neq l$) in nature. We must have the states $|l,\vec{k}\rangle$ initially occupied and $|l',\vec{k}'\rangle$ unoccupied. Equation (1) already embodies the mechanism of plasmon decay excitation of SE's. To see this, we note that the q^{-4} factor implies that transitions involving small momentum transfers are heavily favored. In the limit of very small q and for the NFE metals like Al, ϵ_1 can be regarded as very small in the immediate vicinity of the $q\approx 0$ plasmon frequency ω_p. Hence $|1/\epsilon| = |1/(\epsilon_1+i\epsilon_2)|$ has a large resonance in this domain for ϵ_2 sufficiently small. To put this in mathematical terms we follow Ehrenreich[29] and write

$$\epsilon(q,\omega)\big|_{\omega\approx\omega_p} \approx \left(\epsilon_1(q,\omega_p)+\frac{\partial\epsilon_1}{\partial\omega}\bigg|_{\omega\approx\omega_p}(\omega-\omega_p)+i\epsilon_2(q,\omega_p)\right). \tag{3}$$

Furthermore, for solids like Al, $\lim_{q\to 0}\epsilon_1(q,\omega)$ in the vicinity of ω_p is extremely well approximated by the expression $1-(\omega_p/\omega)^2$. Substituting in (3), we obtain for q small,

$$\epsilon(q,\omega\approx\omega_p)\approx(2/\omega_p)(\omega-\omega_p)+i\epsilon_2(q,\omega_p) \tag{4}$$

and

$$\frac{1}{|\epsilon(q,\omega\approx\omega_p)|^2}\approx\frac{(\omega_p/2)^2}{(\omega-\omega_p)^2+(\omega_p^2/4)\epsilon_2(q,\omega_p)^2}. \tag{5}$$

Defining $\Gamma_v=\lim_{q\to 0}\hbar\omega_p\epsilon_2(q,\omega_p)$, we have

$$\frac{1}{|\epsilon(q,\omega\approx\omega_p)|^2}\approx\frac{(\Gamma_v/2\hbar)(\omega_p/2)}{[(\omega-\omega_p)^2+(\Gamma_v/2\hbar)^2]\epsilon_2(q,\omega_p)}. \tag{6}$$

For Γ_v very small, (6) is a very sharp Lorentzian centered at ω_p, representing the sharp plasmon-loss lines observed in characteristic energy-loss experiments. Γ_v is associated with the finite damping of the plasmons which must exist in actual solids. We note that our expression for Γ_v has already been derived by Pines[14,18] and Ferrell.[19] Substituting (6) into (1), we have, restricting ourselves to processes involving very small q and occurring in the neighborhood of ω_p,

$$W(l\vec{k}\to l'\vec{k}')\approx\left(\frac{32\pi^3e^4}{\Delta^2\hbar q^4}\right)\frac{(\omega_p\Gamma_v/4\hbar)|(l'\vec{k}'|l\vec{k})|^2\delta_{\vec{k}',\vec{k}+\vec{q}}\,\delta(E_{l'\vec{k}'}-E_{l\vec{k}}-\hbar\omega)}{[(\omega-\omega_p)^2+(\Gamma_v/2\hbar)^2]\epsilon_2(q,\omega)}. \tag{7}$$

In (7) we have replaced ω_p by ω in ϵ_2 since we are interested in the frequency region $\omega \approx \omega_p$. Now in the limit of very small q, the RPA expression for $\epsilon_2(\vec{q},\omega)$ in the Bloch scheme can be written as[14,27]

$$\epsilon_2(\vec{q},\omega) = \frac{4\pi^2 e^2}{\Delta q^2} \sum_{l\vec{k}} \delta(\hbar\omega - E_{l,\vec{k}+\vec{q}} + E_{l,\vec{k}}) + \frac{4\pi^2 e^2}{\Delta m^2 \omega^2} \sum_{l'l\vec{k}}{}' |P^{\mu}_{l'l}|^2 \delta(E_{l'\vec{k}'} - E_{l\vec{k}} - \hbar\omega), \tag{8}$$

where

$$P^{\mu}_{l'l} = \frac{1}{\Delta_0} \int_0 u^*_{l'\vec{k}'} \hat{q}\cdot\vec{p} u_{l\vec{k}} d\vec{r}. \tag{9}$$

In (9), $\hat{q} = \vec{q}/q$ and $\vec{p}$ is the momentum operator. The prime on the second summation denotes that terms with $l = l'$ are to be excluded. The first term on the right-hand side in (8) represents the intraband transitions while the second term represents the interband transitions. From perturbation theory,[27] we have

$$\lim_{q\to 0} |(l'\vec{k}'|l,\vec{k}'-\vec{q})|^2 = \delta_{l'l} + (1-\delta_{l'l}) \times \left(\frac{q}{m\omega_{l'l}}\right)^2 |P^{\mu}_{l'l}|^2, \tag{10}$$

where

$$\hbar\omega_{l'l} = E_{l'\vec{k}'} - E_{l\vec{k}}.$$

Using (10) we can write, for q very small,

$$\delta_{\vec{k}',\vec{k}+\vec{q}} |(l'\vec{k}'|l\vec{k})|^2 \delta(E_{l'\vec{k}'} - E_{l,\vec{k}} - \hbar\omega) \approx \delta_{\vec{k}',\vec{k}+\vec{q}} \Big[\delta(E_{l'\vec{k}'} - E_{l',\vec{k}'-\vec{q}} - \hbar\omega)\delta_{l'l} + (1-\delta_{l'l})\left(\frac{q}{m\omega_{l'l}}\right)^2 |P^{\mu}_{l'l}|^2 \times \delta(E_{l'\vec{k}'} - E_{l\vec{k}} - \hbar\omega)\Big]. \tag{11}$$

We now note that for NFE metals like Al, with near parabolic energy bands, the intraband transition energy δ functions in (11) and (8) will, in general, vanish in the limit $q \to 0$ and for $\omega \approx \omega_p$. This is because for near parabolic bands, momentum and energy cannot be conserved simultaneously in this limit. Hence, keeping only the vertical interband transition terms in (11) and (8), and substituting in (7), we have

$$\lim_{q\to 0} W(l\vec{k} \to l'\vec{k}') \approx \left(\frac{4\pi e^2\omega_p}{\Delta\hbar q^2}\right) \frac{\Gamma_v/2\hbar}{(\omega-\omega_p)^2 + (\Gamma_v/2\hbar)^2} \frac{\delta_{\vec{k}',\vec{k}}(1-\delta_{l'l}) f_0(E_{l\vec{k}})[1-f_0(E_{l'\vec{k}'})]|P^{\mu}_{l'l}|^2 \delta(E_{l'\vec{k}'} - E_{l\vec{k}} - \hbar\omega)}{\sum'_{l'l\vec{k}'} f_0(E_{l\vec{k}})[1-f_0(E_{l'\vec{k}'})]|P^{\mu}_{l'l}|^2 \delta(E_{l'\vec{k}'} - E_{l\vec{k}} - \hbar\omega)}. \tag{12}$$

In (12) we have taken care of the occupancy requirements by introducing the Fermi-Dirac distribution functions f_0's. We obtain the total transition rate into final state $|l'\vec{k}'\rangle$ by summing over all $|l,\vec{k}\rangle$ and small wave vectors $\vec{q}$,

$$W_T(l'\vec{k}') = \sum_{\text{small } q\text{'s}} \left(\frac{4\pi e^2\hbar\omega_p}{\Delta\hbar q^2}\right) \frac{\Gamma_v/2}{(\hbar\omega - \hbar\omega_p)^2 + (\Gamma_v/2)^2} \frac{\sum'_l f_0(E_{l\vec{k}'})[1-f_0(E_{l'\vec{k}'})]|P^{\mu}_{l'l}|^2 \delta(E_{l'\vec{k}'} - E_{l\vec{k}} - \hbar\omega)}{\sum'_{l'l\vec{k}'} f_0(E_{l\vec{k}})[1-f_0(E_{l'\vec{k}'})]|P^{\mu}_{l'l}|^2 \delta(E_{l'\vec{k}'} - E_{l\vec{k}} - \hbar\omega)}. \tag{13}$$

From (13), we obtain at once the differential transition rate per unit excited SE energy.

$$\frac{dW}{dE} = \sum_{\text{small } q\text{'s}} \left(\frac{4\pi e^2\hbar\omega_p}{\Delta\hbar q^2}\right) \frac{\Gamma_v/2}{(\hbar\omega - \hbar\omega_p)^2 + \Gamma_v/2)^2} F(E, \hbar\omega),$$

where

$$F(E,\hbar\omega) = \frac{\sum'_{l'l\vec{k}'} f_0(E_{l\vec{k}'})[1-f_0(E_{l'\vec{k}'})]|P^{\mu}_{l'l}|^2 \delta(E_{l'\vec{k}'} - E_{l\vec{k}'} - \hbar\omega)\delta(E_{l'\vec{k}'} - E)}{\sum'_{l'l\vec{k}'} f_0(E_{l\vec{k}})[1-f_0(E_{l'\vec{k}'})]|P^{\mu}_{l'l}|^2 \delta(E_{l'\vec{k}'} - E_{l\vec{k}'} - \hbar\omega)}. \tag{14}$$

We note that for polycrystalline solids or solids with cubic symmetry such as Al, *in the limit* $q \to 0$, the momentum matrix elements are independent of the orientation of $\hat{q}$,[14,29] and the term $F(E,\hbar\omega)$ is identical to the normalized optical energy distribution of the joint density of states encountered in photoemission studies of solids.[30]

Now in (14) the factor

$$\sum_{\text{small } q\text{'s}} \frac{4\pi e^2 \hbar\omega_p(\Gamma_v/2)}{\Delta\hbar q^2[(\hbar\omega-\hbar\omega_p)^2+(\Gamma_v/2)^2]}$$

is just the transition rate for generating long-wavelength plasmons. Also the term $F(E,\hbar\omega)$ is correctly interpreted as the electron energy distribution resulting from plasmon decay via vertical interband transitions. Hence (14), (13), and (12) describe a second-order process in which the incident electron first creates plasmons with $q \approx 0$ which subsequently decay via vertical interband transitions, thereby producing energetic SE's.

To proceed further, we replace the summation in $\vec{q}$ by an integral,

$$\sum_{\vec{q}} \to \frac{\Delta}{8\pi^3}\int d\vec{q}\,.$$

Referring to Fig. 1, which depicts the geometry of the scattering act, we have $d\vec{q} = 2\pi q_\perp dq_\perp dq_{\parallel}$. Also, for very small q or, equivalently, θ, we have the approximate relation[16]

$$q^2 = q_\perp^2 + q_{\parallel}^2 \approx K_0^2(\theta^2+\theta_E^2), \tag{15}$$

where $\theta_E = \hbar\omega/2E_0$, and E_0 is the incident electron energy. Hence,

$$d\vec{q} \approx \pi K_0^3 \theta\, d\theta\, d(\hbar\omega)/E_0\,. \tag{16}$$

Substituting in (14), we have

$$\frac{dW_T}{dE} = \frac{e^2\hbar\omega_p K_0}{2\hbar E_0} \times \int_0^{\theta_1} \frac{\theta\, d\theta}{\theta^2+\theta_E^2} \times \int_0^{\infty} d(\hbar\omega) \times \left(F(E,\hbar\omega)\frac{\Gamma_v/2\pi}{(\hbar\omega-\hbar\omega_p)^2+(\Gamma_v/2)^2}\right). \tag{17}$$

Dividing (17) by the incident-electron velocity,

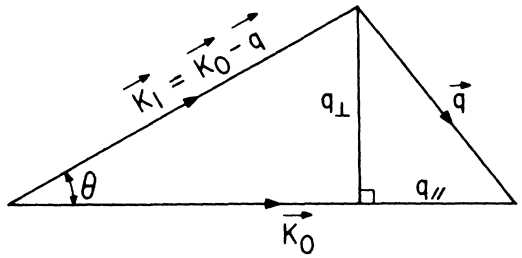

FIG. 1. Scattering geometry discussed in the text. $\vec{K}_0$ and $\vec{K}_1$ are initial and final wave vectors of the incident primary electron. The components of the momentum transferred parallel and perpendicular to $\vec{K}_0$ are denoted by $\hbar q_{\parallel}$ and $\hbar q_\perp$ respectively.

we obtain the differential inverse mean free path (MFP), or probability per unit distance for creating SE's by volume-plasmon decay,

$$\frac{d(1/\lambda)}{dE} = \lambda_{\text{eff}}^{-1}(E_0,\theta_1)\int_0^{\infty} F(E,\hbar\omega) \times \frac{1}{\pi}\left[\frac{\Gamma_v/2}{(\hbar\omega-\hbar\omega_p)^2+(\Gamma_v/2)^2}\right] d(\hbar\omega)\,, \tag{18}$$

where

$$\lambda_{\text{eff}}(E_0,\theta_1) = \frac{2a_0E_0}{\hbar\omega_p}\left[\ln\left(\frac{\theta_1^2+\theta_E^2}{\theta_E^2}\right)^{1/2}\right]^{-1}, \tag{19}$$

with $a_0 = \hbar^2/me^2$ the first Bohr radius.

In (18) and (19), $\lambda_{\text{eff}}(E_0,\theta_1)$ is the effective MFP for creating long-wavelength plasmons, θ_1 being a small upper limit of integration so that the maximum wave vectors of the plasmons considered in (18), $q_1 = K_0(\theta_1^2+\theta_E^2)^{1/2}$, is very small compared with typical Brillouin-zone dimensions ($\sim 1\,\text{Å}^{-1}$). In this way, we can characterize the interband transitions causing plasmon decay as approximately vertical in nature.

Specializing to the case of Al, we can evaluate the energy distribution of the joint density of states $F(E,\hbar\omega)$, using the simple two-band (or two-orthogonalized-plane-wave in Harrison's[31] terminology) model used by previous workers to analyze the optical properties of this metal.[30,32] From the work of Koyama and Smith,[30] we can easily derive the following expression for $F(E,\hbar\omega)$ in the two-band model:

$$F(E,\hbar\omega) = \frac{\sum_{\vec{G}} n_{\vec{G}}^{\vec{}}\, G\,|W_{\vec{G}}^{\vec{}}|^2[H(E-E_1^G-\hbar\omega)-H(E-E_F-\hbar\omega)]}{\sum_{\vec{G}} n_{\vec{G}}^{\vec{}}\, G\,|W_{\vec{G}}^{\vec{}}|^2(E_F-E_1^G)}, \tag{20}$$

where

$$E_1^G = \frac{(\hbar\omega - \hbar^2G^2/2m)^2 - 4|W_{\vec{G}}|^2}{2\hbar^2G^2/m}. \quad (21)$$

In (20), we sum over all nonequivalent reciprocal-lattice vectors $\vec{G}$ corresponding to the distinct Bragg planes capable of causing vertical interband transitions at $\hbar\omega$. Also $n_{\vec{G}}$ is the number of equivalent reciprocal-lattice vectors corresponding to $\vec{G}$, $W_{\vec{G}}$ is the $\vec{G}$th Fourier coefficient of the lattice pseudopotential, $H(x)$ is the unit step function, and E_F is the Fermi energy. In (20), (21), and all subsequent analysis in this paper, the electron zero of energy is set at the bottom of the conduction band unless stated otherwise. For Al, Ashcroft and Sturm,[32] and Koyama and Smith[30] found that by using the two-band model, good results are obtained by considering only the eight equivalent reciprocal-lattice vectors $\vec{G}_{111}$ and the six equivalent vectors $\vec{G}_{200}$. We shall follow Refs. 30 and 32 and only sum over $\vec{G}_{111}$ and $\vec{G}_{200}$ in (20) for Al with $n_{111}=8$ and $n_{200}=6$. Finally, substituting (20) into (18), we obtain

$$\frac{d(1/\lambda)}{dE} = \lambda_{\text{eff}}^{-1}(E_0, \theta_1)D(E, \hbar\omega_p, \Gamma_v), \quad (22)$$

where

$$D(E,\hbar\omega_p,\Gamma_v) = \left\{\sum_{\vec{G}} n_{\vec{G}} G|W_{\vec{G}}|^2\left[\tan^{-1}\left(\frac{E-E_0^G-\hbar\omega_p}{\Gamma_v/2}\right) - \tan^{-1}\left(\frac{E-E_F-\hbar\omega_p}{\Gamma_v/2}\right)\right]\right\} \times\left\{\pi\sum_{\vec{G}} n_{\vec{G}} G|W_{\vec{G}}|^2(E_F-E_0^G)\right\}^{-1} \quad (23)$$

and

$$E_0^G = E_1^G(\omega=\omega_p) = \frac{(\hbar\omega_p - \hbar^2G^2/2m)^2 - 4|W_{\vec{G}}|^2}{2\hbar^2G^2/m}. \quad (24)$$

In arriving at (22)–(24), we have made use of the fact that since the Lorentzian in (18) is sharply peaked at $\omega=\omega_p$ for small Γ_v, it is a good approximation to set $\omega=\omega_p$ in the expression for E_1^G entering $F(E,\hbar\omega)$, making the integration in (18) elementary. It is easily shown the $\int D(E,\hbar\omega_p,\Gamma_v)\,dE = 1$, as it should since $D(E,\hbar\omega_p,\Gamma_v)$ describes plasmon decay via one-electron transitions.

Before we conclude the present section, the following remarks are in order. First, the vertical interband transitions giving rise to (20)–(24) are the so-called normal or Butcher-type transitions discussed extensively within the context of the optical conductivity of NFE metals.[32-34] Second, our discussion of plasmon decay via interband transitions is based on the dipole or long-wavelength approximation to $\epsilon_2(\vec{q},\omega)$ [cf. Eqs. (8), (10), and (14)]. Such an approximation is valid for plasmon wave vectors such that $qa \ll 2\pi$ or, equivalently, $\lambda \gg a$, where λ is the plasmon wavelength ($\lambda = 2\pi/q$) and a is the unit-cell dimension. Actually, the dipole approximation should be reasonably valid for $\lambda \gtrsim 10a$.[35] However, q cannot be less than the minimum value determined by the primary-electron scattering geometry. Specifically $q \geq q_0 = K_0\theta_E$ [cf. Eq. (15)] for the small-angle case. For the dipole approximation to be valid, we must have $q_0 \leq q \leq q_1 \ll 2\pi/a$, where q_1 is the maximum plasmon wave number considered. In the case of Al, for E_0 (incident primary energy) = 1 keV (the range of values used in the experiments to which we shall compare our theoretical results in Sec. VI, $q_0 \simeq 0.15$ Å^{-1}. In our subsequent calculations for Al, we have decided to set $q_1 = 0.2$ Å^{-1}, slightly larger than the minimum value permissible at $E_0 = 1$ keV. (Since 1 keV is the minimum value of E_0 used in our calculations and since $q_0 \propto E_0^{-1/2}$, this value of q_1 is always greater than q_0.) Now in Al, $a \simeq 3$ Å; hence for $q_1 = 0.2$ Å^{-1}, we have $q_1 \approx (2\pi/a)\times 10^{-1}$ or $\lambda_1 \approx 10a$, where $\lambda_1 = 2\pi/q_1$ is the minimum plasmon wavelength considered. Hence, for our choice of q_1, the dipole approximation on which our treatment of plasmon decay is based is expected to be reasonably valid.

III. SE EXCITATION: SCREENED ELECTRON-ELECTRON SCATTERING

In this section, we analyze the direct excitation of SE's via screened electron-electron scattering between the incident primary and crystal electrons. This process is also contained in Eq. (2) of Sec. II. We rewrite (2) in the following form:

$$W(l\vec{k} \to l'\vec{k}') = \frac{32\pi^3e^4|(l'\vec{k}'|l\vec{k})|^2 f_0(E_{l\vec{k}})[1-f_0(E_{l'\vec{k}'})]\delta_{\vec{k}',\vec{k}+\vec{q}}\,\delta(E_{l'\vec{k}'} - E_{l\vec{k}} - \hbar\omega)}{\Delta^2\hbar q^4|\epsilon(\vec{q},\omega)|^2}. \quad (25)$$

In treating the direct electron-electron interaction process, we must ignore the plasmon pole contribution to $|1/\epsilon(\vec{q},\omega)|^2$ in evaluating (25). This is because we have already considered the plasmon resonance in Sec. II.

Although the Bloch form of the RPA to $\epsilon(\vec{q},\omega)$ is explicitly known,[14,27] it is not very practical to calculate (25) as it stands since one would have to calculate the actual band structure, and evaluate the matrix elements $(l'\vec{k}'\,|\,l\vec{k})$ and $\epsilon(\vec{q},\omega)$, etc. Instead, we have chosen to evaluate the direct electron-electron interaction contribution by using the jellium or free-electron-gas model to describe the valence electrons. We expect this to be fairly reasonable approximation for Al since its calculated band structure is so nearly free-electron-like.[31] In the free-electron-gas picture, the RPA expression for $\epsilon(\vec{q},\omega)$ becomes the well-known Lindhard dielectric function.[14] Furthermore, we shall simplify matters by using the static, long-wavelength form of the Lindhard dielectric function,[14] $\lim_{q\to 0}\epsilon_L(\vec{q},0)=1+(q_{FT}/q)^2$, where q_{FT} is the Thomas-Fermi screening wave vector. This should be a good approximation for the excitation of very-low-energy SE's.

In the jellium model, the crystal electrons are described by plane waves and occupy a Fermi sea (or sphere) in $\vec{k}$ space at absolute-zero temperature. Hence in (25), $(l'\vec{k}'\,|\,l\vec{k})$ is replaced by unity. Dropping the l and l', we obtain

$$W(\vec{k}\to\vec{k}') = \frac{32\pi^3 e^4 f_0(E_{\vec{k}})[1-f_0(E_{\vec{k}'})]\delta_{\vec{k}',\vec{k}+\vec{q}}\,\delta(E_{\vec{k}'}-E_{\vec{k}}-\hbar\omega)}{\Delta^2\hbar(q^2+q_{FT}^2)^2}. \tag{26}$$

We have used the expression $\lim_{q\to 0}\epsilon_L(\vec{q},0)=1+(q_{FT}/q)^2$ in (26). The total transition rate for generating SE's of wave vector $\vec{k}'$ is

$$W_T(\vec{k}') = \sum_{\vec{q},\vec{k}} W(\vec{k}\to\vec{k}') = \sum_{\vec{q}} \frac{32\pi^3 e^4 f_0(E_{\vec{k}'-\vec{q}})[1-f_0(E_{\vec{k}'})]\delta(E_{\vec{k}'}-E_{\vec{k}'-\vec{q}}-\hbar\omega)}{\Delta^2\hbar(q^2+q_{FT}^2)^2}, \tag{27}$$

where

$$\hbar\omega=\frac{\hbar^2K_0^2}{2m}-\frac{\hbar^2(\vec{K}_0-\vec{q})^2}{2m},$$

$$E_{\vec{k}'}=\frac{\hbar^2k'^2}{2m},\quad E_{\vec{k}'-\vec{q}}=\frac{\hbar^2(\vec{k}'-\vec{q})^2}{2m}.$$

The summation in (27) can be carried out exactly. In Appendix B we give an outline of the calculations involved. The final result is simply stated below,

$$W_T(\vec{k})=\frac{2\pi me^4}{\Delta\hbar^3|\vec{K}_0-\vec{k}|q_{FT}^2}\left\{1-(k^2-k_F^2+q_{FT}^2)\left[(k^2-k_F^2)^2+2q_{FT}^2\left(k^2+k_F^2-\frac{2|\vec{k}\cdot(\vec{K}_0-\vec{k})|^2}{|\vec{K}_0-\vec{k}|^2}\right)+q_{FT}^4\right]^{-1/2}\right\} \tag{28}$$

for $|\vec{k}\cdot(\vec{K}_0-\vec{k})|\le k_F|\vec{K}_0-\vec{k}|$, $k\ge k_F$; and $W_T(\vec{k})=0$, otherwise.

In (28) we have relabeled $\vec{k}'$ by $\vec{k}$ and k_F is the Fermi wave vector. Dividing (28) by the incident-electron velocity and summing over $\vec{k}$, we obtain the total inverse MFP for screened electron-electron scattering,

$$1/\lambda=\sum_{\vec{k}}\frac{m}{\hbar K_0}W_T(\vec{k}) = \frac{\Delta}{4\pi^3}\int\frac{m}{\hbar K_0}W_T(\vec{k})k^2\,dk\,d\Omega_{\vec{k}}. \tag{29}$$

Using the relations $E=\hbar^2k^2/2m$, $k^2\,dk=(m/\hbar^3)(2mE)^{1/2}\,dE$, specializing to the important case of very high incident-electron energy and low excited-SE energy such that we can set $\vec{K}_0-\vec{k}\approx\vec{K}_0$, we obtain from (29) and (28), after some algebra,

$$\frac{d^2(1/\lambda)}{dE\,d\Omega_\gamma}=\Re\,\frac{q_{FT}E^{1/2}}{4\pi^2E_0E_{FT}^{3/2}}\left(1-\frac{E-E_F+E_{FT}}{[(E-E_F)^2+2E_{FT}(E+E_F-2E\cos^2\gamma)+E_{FT}^2]^{1/2}}\right). \tag{30}$$

In (30), $\Re=e^2/2a_0$ is the Rydberg constant, $E_{FT}=\hbar^2q_{FT}^2/2m$, E_F is the Fermi energy, and γ is the angle between $\vec{k}$ and $\vec{K}_0$. Also in (29) and (30), $d\Omega_\gamma$ is a differential solid angle in the direction of γ.

By integrating (30) over $d\Omega_\gamma$, we have

$$\frac{d(1/\lambda)}{dE}=2\pi\int_{-k_F/k}^{k_F/k}\frac{d^2(1/\lambda)}{dE\,d\Omega_\gamma}\,d(\cos\gamma) = (2\pi E_0\Re\beta^3k_F^3a_0^4)^{-1}\left[2\beta E_F-(E-E_F+E_{FT})\sin^{-1}\left(\frac{2\beta E_F}{[(E-E_F)^2+2E_{FT}(E+E_F)+E_{FT}^2]^{1/2}}\right)\right], \tag{31}$$

for $E_0 \gg E$, where $\beta = q_{FT}/k_F$.

Equations (28), (30), and (31) give the various SE excitation functions arising from direct electron-electron scattering, taking into account static screening only. An investigation of (30) revealed that for large E_0 ($\gtrsim 1$ keV) and low SE energy E ($\lesssim 100$ eV), $d^2(1/\lambda)/dE\, d\Omega_\gamma \sim \sin^2\gamma$. We can write, in this regime,

$$\frac{d^2(1/\lambda)}{dE\, /d\Omega_\gamma} \simeq Q(E) \sin^2\gamma,$$

where

$$\frac{d(1/\lambda)}{dE} \simeq Q(E) \int_0^\pi 2\pi \sin^3\gamma\, d\gamma \simeq \frac{8\pi}{3} Q(E). \tag{32}$$

Hence for large E_0 and small E, we have the approximate relation

$$\frac{d^2(1/\lambda)}{dE\, d\Omega_\gamma} \simeq \frac{3}{8\pi} \frac{d(1/\lambda)}{dE} \sin^2\gamma. \tag{33}$$

Equations (31) and (32) will be used later in our quantitative calculations for Al. As a reviewer has pointed out, it is not rigorously correct to use the Fermi-Thomas (static) approximation when the excited SE's have final energies far from the Fermi surface. However, the results obtained in the present section are not entirely without justifications. In the footnote under Ref. 36, we present some arguments in favor of our results based on the static approximation.

IV. SE EXCITATION: SURFACE-PLASMON DECAY

In this section, we investigate the possible role played by surface-plasmon decay in SEE in solids. We again restrict ourselves to plasmons of small wave vectors. The physical picture is the same as in the case of volume-plasmon decay. We have an incident fast electron exciting a surface plasmon on the metal-vacuum interface which subsequently decays into single-electron transitions. We consider the case of a semi-infinite solid situated in vacuum. The coupling of fast electrons with surface plasmons was first treated by Ritchie.[37] Neglecting hydrodynamic dispersion and retardation effects,[38] Stern and Ferrell[39] have given a simple derivation of the probability of exciting surface plasmons by incident electrons for a semi-infinite NFE solid. For normal incidence of the external fast electron, Stern and Ferrell have obtained the following result[39]:

$$\frac{dP}{d\Omega_\theta} = \frac{e^2 \theta_{ES} \theta}{\pi \hbar v_0 (\theta^2 + \theta_{ES}^2)^2}. \tag{34}$$

In (34), θ is the scattering angle (see Fig. 2), $\theta_{ES} = \hbar\omega_s/2E_0$ ($\hbar\omega_s$ is the nominal surface-plasmon energy), and v_0 is the incident-electron velocity. $dP/d\Omega_\theta$ is the differential probability per unit solid angle for creating a surface plasmon. In arriving at (34), the small-θ approximation has been made and surface-plasmon dispersion is ignored. We have $\hbar\omega_s = \hbar\omega_p/\sqrt{2}$.

Neglecting retardation and hydrodynamic dispersion effects, the surface-plasmon field can be described by a simple scalar electric potential.[39] For a semi-infinite solid bounded by vacuum, one can write

$$\phi_s(\vec{r}, t) = \sum_{\vec{Q}} \phi_0(\vec{Q}) e^{i(\vec{Q}\cdot\vec{s} - \omega_s t)} e^{-Q|z|}. \tag{35}$$

In (35) $\vec{s} = \hat{x}x + \hat{y}y$ is the position coordinate parallel to the surface and z is the coordinate normal to it. The solid is situated in the half-space $z > 0$, with the solid-vacuum interface at $z = 0$. $\vec{Q}$ is the two-dimensional wave vector of the surface-plasmon field, i.e., $\vec{Q} = Q_x\hat{x} + Q_y\hat{y}$. Since the surface-plasmon field decays exponentially into the solid, one can have excitation of the bulk-crystal electrons via coupling to the electric potential $\phi_s(\vec{r}, t)$. Endriz and Spicer[40] have discussed a so-called surface-plasmon-decay volume photoemission effect in Al. In their case, the surface plasmons are excited by photons which are coupled to the surface-plasmon field through surface roughness. We shall follow Endriz and Spicer's analysis (see Sec. II A of Ref. 40) in our treatment of SE excitation via surface-plasmon decay.

Following Ref. 40, we can assume that each $\vec{Q}$th component of the surface-plasmon potential has a field energy distribution into the solid given

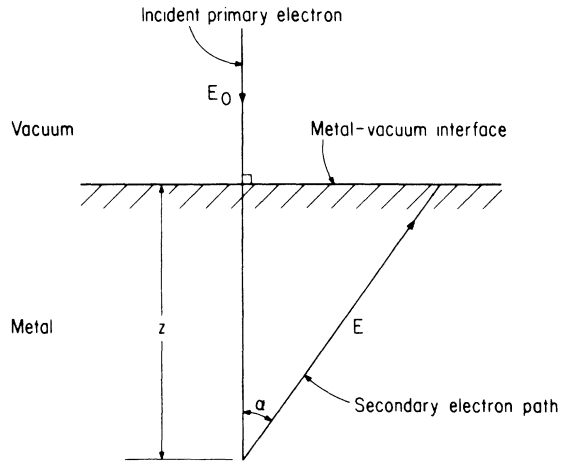

FIG. 2. Diagram illustrating the escape of unscattered secondary electrons. E_0 and E are the primary- and excited-secondary-electron energies, respectively. Also, z is the distance into the solid at which the secondary electron is created, while α is the angle specifying direction of escape of the excited secondary electron.

by e^{-2Qz} ($z>0$). If it is assumed that single-electron excitation is the principal plasmon decay mechanism, we can assume that the probability per unit distance of exciting SE's is given by $2Qe^{-2Qz}$. If $F(E,\hbar\omega_s)$ is the normalized energy distribution of surface-plasmon decay via single-electron excitation, we can write the differential probability per unit distance per unit energy of SE excitation via this process as

$$\frac{d\lambda^{-1}(z)}{dE}=2Qe^{-2Qz}F(E,\hbar\omega_s). \tag{36}$$

For polycrystalline or cubic solids (e.g., Al) and for very small Q's it is not hard to show, using the same arguments in Sec. II, that $F(E,\hbar\omega_s)$ is just the normalized optical energy distribution of the joint density of states for vertical interband transitions defined by (20) and (21). Equation (36) describes a volume SE excitation process analogous to conventional volume photoexcitation. As Endriz and Spicer[40] have pointed out, $2Q$ here plays the role of the photon absorption coefficient.

Convolving (36) with a Lorentzian, as in Sec. II, to account for plasmon lifetime broadening, we obtain

$$\frac{d\lambda^{-1}(z)}{dE}=2Qe^{-2Qz}D(E,\hbar\omega_s,\Gamma_s), \tag{37}$$

where $D(E,\hbar\omega_s,\Gamma_s)$ is the same function defined in (23) but with parameters appropriate to surface plasmons. Multiplying (37) by (34) we obtain the double differential inverse MFP for SE excitation via decay of surface plasmons of wave vector Q:

$$\frac{d^2\lambda^{-1}(z)}{dE\,d\Omega_\theta}=\frac{e^2\theta_{ES}\theta}{\pi\hbar v_0(\theta^2+\theta_{ES}^2)^2}\,2K_0\theta e^{-2K_0\theta z}D(E,\hbar\omega_s,\Gamma_s). \tag{38}$$

In (38), we have equated Q with $K_0\theta$ from consideration of the scattering geometry for small θ. $d\Omega_\theta$ is a differential solid angle about the scattering angle θ.

V. SE TRANSPORT AND ESCAPE

In our treatment of the SE transport and escape problem we shall only consider those SE's that do not suffer any scattering on their way to the surface and those that scatter only once. Our analysis is largely based on the original work of Berglund and Spicer[41] in connection with photoemission. Following previous work in SEE[3,5,10,42] the only scattering process that we shall consider is inelastic electron-electron scattering. [We shall ignore electron-phonon (elastic) scattering since there does not appear to be any appreciable temperature dependence in SEE in metals. Our SE transport model is based on a similar one used earlier by us in a simple calculation of SEE,[10] but represents an extension of that work by considering once-scattered electrons also.

A. Unscattered SE's: Volume-plasmon decay and direct electron-electron interaction

We consider a primary electron incident normally on a semi-infinite solid situated in vacuum. We assume that the primary-electron energy is sufficiently high so that we can approximate its trajectory throughout a typical low-energy SE escape depth (~50 Å in most metals) as a straight line. This is an often used assumption in many phenomenological theories of SEE in solids for high primary energies.[12,13] The treatment of the unscattered SE's for the contributions from volume-plasmon decay and direct electron-electron interaction is particularly simple. Using the idealized step-potential model of the solid-vacuum surface barrier and an escape-cone argument, we can write for the external energy distribution of emitted unscattered SE's

$$N_0(E)=\int_0^d\int_0^{2\pi}\int_0^{\alpha_c(E)}\frac{d^2(1/\lambda)}{dE\,d\Omega_\alpha}e^{-z/l(E)\cos\alpha}\times\sin\alpha\,d\alpha\,d\phi\,dz\,. \tag{39}$$

Referring to Fig. 2, α is the polar angle specifying the initial direction of motion of the SE of energy E created at depth z. ϕ is the azimuthal angle and $d\Omega_\alpha$ is an element of solid angle centered at the angular coordinates (α,ϕ). In (39), $l(E)$ is the energy-dependent inelastic electron-electron scattering MFP, $d^2(1/\lambda)/dE\,d\Omega_\alpha$ is the double differential inverse MFP for excitation of SE's by either volume-plasmon decay (Sec. II) or direct electron-electron scattering (Sec. III). Also, d is a maximum phenomenological SE escape depth, and $\alpha_c(E)$ is a maximum emission angle such that the normal component of momentum is just enough to surmount the surface barrier,

$$\alpha_c(E)=\cos^{-1}\{[(E_F+\phi)/E]^{1/2}\}, \tag{40}$$

where ϕ is the work function. [We are assuming that the excited SE's are treated as free electrons in arriving at (40) and in all subsequent analysis.]

For the contribution from volume-plasmon decay, we assume that the excited SE's are distributed isotropically. Such an assumption is probably permissible in a first-order treatment such as the present one. Hence, for volume-plasmon decay,

$$\left(\frac{d^2(1/\lambda)}{dE\,d\Omega_\alpha}\right)_{VP}=\frac{1}{4\pi}\left(\frac{d(1/\lambda)}{dE}\right)_{VP},$$

$$[N_0(E)]_{VP}=\frac{1}{2}\int_0^d\int_0^{\alpha_c(E)}\lambda_{eff}^{-1}(E_0,\theta_1)D(E,\hbar\omega_p,\Gamma_v)\times e^{-z/l(E)\cos\alpha}\sin\alpha\,d\alpha\,. \tag{41}$$

In (41), we have made use of (22). Now following previous work,[10] we assume the primary energy E_0 remains constant throughout a distance d and take λ_{eff}^{-1} outside the integral signs. Also noting[10] that since $e^{-z/l(E)\cos\alpha}$ is a rapidly decreasing function of z, we make the approximation of replacing d by ∞, so that

$$[N_0(E)]_{VP}=\tfrac{1}{2}\lambda_{eff}^{-1}(E_0,\theta_1)D(E,\hbar\omega_p,\Gamma_v)\times\int_0^\infty\int_0^{\alpha_c(E)}e^{-z/l(E)\cos\alpha}\sin\alpha\,d\alpha$$

$$=\tfrac{1}{4}\lambda_{eff}^{-1}(E_0,\theta_1)D(E,\hbar\omega_p,\Gamma_v)l(E)\left(1-\frac{E_F+\phi}{E}\right). \tag{42}$$

An equation similar to (42) but involving Streitwolf's unscreened result has already been derived earlier by the present authors.[10]

For the contribution from direct electron-electron scattering, we have from (33)

$$\left(\frac{d^2(1/\lambda)}{dE\,d\Omega_\alpha}\right)_{ee}=\left(\frac{d^2(1/\lambda)}{dE\,d\Omega_\gamma}\right)_{ee}\Bigg|_{\gamma=\pi-\alpha}\simeq\frac{3}{8\pi}\left(\frac{d(1/\lambda)}{dE}\right)_{ee}\sin^2\alpha\,, \tag{43}$$

where $[d(1/\lambda)/dE]_{ee}$ is defined by (31).

Making the same approximations as before, we obtain

$$[N_0(E)]_{ee}\simeq\frac{3}{4}\left(\frac{d(1/\lambda)}{dE}\right)_{ee}\int_0^\infty\int_0^{\alpha_c(E)}e^{-z/l(E)\cos\alpha}\sin^3\alpha\,d\alpha\,dz$$

$$\simeq\frac{3}{16}\left(\frac{d(1/\lambda)}{dE}\right)_{ee}l(E)\left(1-\frac{E_F+\phi}{E}\right)^2. \tag{44}$$

B. Unscattered SE's: Surface-plasmon decay

For this contribution to the external SE energy distribution, the treatment is slightly different. We start from (39) and using (38), assuming as in the volume-plasmon case that the SE's created by surface-plasmon decay are distributed isotropically, we can write for surface-plasmon decay

$$\frac{d[N_0(E)]_{SP}}{d\Omega_\theta}=\frac{1}{2}\int_0^\infty\int_0^{\alpha_c(E)}\left(\frac{d^2(1/\lambda)}{dE\,d\Omega_\theta}\right)_{SP}e^{-z/l(E)\cos\alpha}\sin\alpha\,d\alpha\,dz$$

$$=\frac{e^2\theta_{ES}K_0\theta^2D(E,\hbar\omega_s,\Gamma_s)}{\pi\hbar v_0(\theta^2+\theta_{ES}^2)^2}\int_0^\infty\int_0^{\alpha_c(E)}\exp\left[-\left(2K_0\theta+\frac{1}{l(E)\cos\alpha}\right)z\right]\sin\alpha\,d\alpha\,dz$$

$$=\frac{\theta_{ES}\theta^2D(E,\hbar\omega_s,\Gamma_s)}{\pi a_0(\theta^2+\theta_{ES}^2)^2}\int_0^{\alpha_c(E)}\left(2K_0\theta+\frac{1}{l(E)\cos\alpha}\right)^{-1}\sin\alpha\,d\alpha\,. \tag{45}$$

In (45), $d\Omega_\theta$ is the differential solid angle about the primary-electron scattering angle θ and should not be confused with the corresponding quantity about the SE emission angle α. Now the integral in (45) can be performed exactly[41] and we can write

$$\frac{d[N_0(E)]_{SP}}{d\Omega_\theta}=\frac{\theta_{ES}\theta^2D(E,\hbar\omega_s,\Gamma_s)C(K_0\theta,E)}{\pi a_0(\theta^2+\theta_{ES}^2)^2}, \tag{46}$$

where

$$C(K_0\theta,E)=\frac{1}{2K_0\theta}\left[2T(E)-\frac{1}{2K_0\theta l(E)}\times\ln\left(\frac{1+2K_0\theta l(E)}{1+2K_0\theta l(E)-4K_0\theta T(E)l(E)}\right)\right],$$

with

$$T(E)=\frac{1}{2}\left[1-\left(\frac{E_F+\phi}{E}\right)^{1/2}\right].$$

From (46), the total unscattered external SE energy distribution arising from surface-plasmon decay is

$$[N_0(E)]_{SP}=2\pi\int_0^{\theta_1}\frac{d[N_0(E)]_{SP}}{d\Omega_\theta}\sin\theta\,d\theta=\frac{2\theta_{ES}D(E,\hbar\omega_s,\Gamma_s)}{a_0}\int_0^{\theta_1}\frac{\theta^3C(K_0\theta,E)\,d\theta}{(\theta^2+\theta_{ES}^2)^2}. \tag{47}$$

In (47), θ_1 is a small upper limit of integration, so that the corresponding surface-plasmon wave vectors are small in the sense discussed in Sec. II.

C. Once-scattered SE's: Volume-plasmon decay and direct electron-electron interaction

In treating the contribution of once-scattered SE's to the external EDC, we shall only consider those SE's excited via volume-plasmon decay and screened electron-electron scattering. This is because the $e^{-2K_0\theta z}$ factor in (38) implies that SE's excited by surface-plasmon decay are generally created nearer to the solid surface and hence have a lesser chance of scattering before emission. This is not a rigorous argument and we could have included once-scattered electrons for this case also, using the formalism of Berglund and Spicer[41] for instance. We have decided not to do so here to simplify our calculations.

In treating once-scattered SE's in the other two cases, we assume, as in Ref. 41, that the electron-electron scattering is spherically symmetric in the laboratory frame. Figure 3 depicts a SE excited at depth z from either volume-plasmon decay or screened electron-electron scattering initially moving with an energy E' at an angle α with the z axis. It travels a distance r, suffers an inelastic electron-electron scattering, and moves off with a final energy E at an angle δ with z axis. Following Ref. 41, we can write for the external energy distribution of once-scattered SE's

$$N_1(E)=\pi\int_E^{E_1}dE'\int_0^{\infty}dz\int_0^{\delta_c(E)}d\delta\left[\left(\int_0^{\pi/2}d\alpha\int_0^{z/\cos\alpha}dr+\int_{\pi/2}^{\pi}d\alpha\int_0^{\infty}dr\right)\right]$$
$$\times\frac{d^2(1/\lambda)}{dE'\,d\Omega_\alpha}e^{-r/l(E')}\frac{dl^{-1}(E')}{dE}e^{-(z-r\cos\alpha)/l(E)\cos\delta}\sin\alpha\sin\delta\ . \tag{48}$$

In (48), $\delta_c(E)=\cos^{-1}\{[(E_F+\phi)/E]\}^{1/2}$ and E_1 is an upper limit of initial SE energy. $dl^{-1}(E')/dE$ is the differential inverse MFP for an excited SE with energy E' to be scattered by electron-electron scattering with the Fermi sea into a final energy between E and $E+dE$.

Carrying out the integrations in r and z in (48) we obtain after setting $x=\cos\alpha$, $y=\cos\delta$, $y_c=[(E_F+\phi)/E]^{1/2}$, and with the same approximations as in the no-scattering case,

$$N_1(E)\simeq\pi\int_E^{E_1}dE'\int_{y_c}^{1}dy\frac{dl^{-1}(E')}{dE}\left[\int_0^1\frac{d^2(1/\lambda)}{dE'\,d\Omega_\alpha}l(E')l(E)y\,dx+\int_{-1}^{0}\frac{d^2(1/\lambda)}{dE'\,d\Omega_\alpha}\left(\frac{l(E')l^2(E)y^2}{l(E)y-l(E')x}\right)dx\right]. \tag{49}$$

To simplify (49) further, we note that for low SE energies l is a strongly decreasing function of energy.[43,44] For $E_1\gg E$ we have $l(E')\ll l(E)$ for at least part of the integration range in E'. Hence we approximate the factor $l(E')l^2(E)y^2/[l(E)y-l(E')x]$ by $l(E')l(E)y$, so that (49) becomes

$$N_1(E)\simeq\pi\int_E^{E_1}dE'\left(\int_{y_c}^{1}\frac{dl^{-1}(E')}{dE}l(E')l(E)y\,dy\times\int_0^{\pi}\frac{d^2(1/\lambda)}{dE'\,d\Omega_\alpha}\sin\alpha\,d\alpha\right)$$
$$\simeq\frac{1}{4}\left(1-\frac{E_F+\phi}{E}\right)l(E)\times\int_E^{E_1}\frac{d(1/\lambda)}{dE'}\frac{dl^{-1}(E')}{dE}l(E')\,dE'\ . \tag{50}$$

In (48)–(50), $d^2(1/\lambda)/dE'\,d\Omega_\alpha$ is the differential inverse MFP for exciting SE's via either volume-plasmon decay (Sec. II) or direct electron-electron interaction (Sec. III);

$$\frac{d(1/\lambda)}{dE'}=2\pi\int\frac{d^2(1/\lambda)}{dE'\,d\Omega_\alpha}\sin\alpha\,d\alpha$$

and is given by (22) or (31), so that (50) is applicable to both processes.

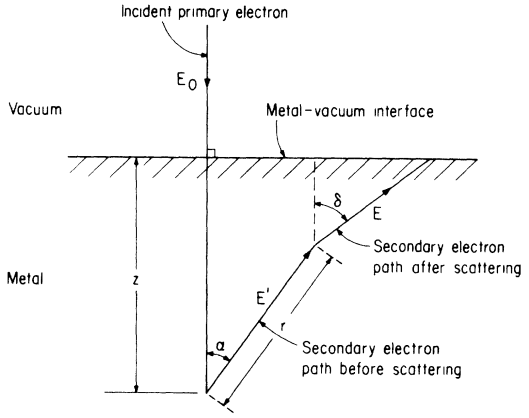

FIG. 3. Diagram illustrating escape of once-scattered secondary electrons. Symbols are explained in Sec. V in the text.

VI. CALCULATIONS FOR ALUMINUM AND COMPARISONS WITH EXPERIMENTAL DATA

Using the formalisms discussed in the previous sections, we have performed quantitative calculations for Al. The total external SE energy distribution is expressed as a sum of three contributions coming from volume-plasmon decay, screened scattering, and surface-plasmon decay, respectively,

$$N(E) = [N(E)]_{VP} + [N(E)]_{ee} + [N_0(E)]_{SP}\,, \tag{51}$$

$$\begin{aligned}[N(E)]_{VP} &= [N_0(E)]_{VP} + [N_1(E)]_{VP} \\ &= \tfrac{1}{4}\lambda_{eff}^{-1}(E_0,\theta_1)D(E,\hbar\omega_p,\Gamma_v)l(E)\left(1-\frac{E_F+\phi}{E}\right) \\ &\quad + \lambda_{eff}^{-1}(E_0,\theta_1)l(E)\left(1-\frac{E_F+\phi}{E}\right) \\ &\quad \times\int_E^{E_1} D(E',\hbar\omega_p,\Gamma_v)\frac{dl^{-1}(E')}{dE}\,l(E')\,dE'\,,\end{aligned} \tag{52}$$

$$\begin{aligned}[N(E)]_{ee} &= [N_0(E)]_{ee} + [N_1(E)]_{ee} \\ &= \frac{3}{16}\left(\frac{d(1/\lambda)}{dE}\right)_{ee} l(E)\left(1-\frac{E_F+\phi}{E}\right)^2 \\ &\quad + \frac{1}{4}\left(1-\frac{E_F+\phi}{E}\right)l(E) \\ &\quad \times\int_E^{E_1}\left(\frac{d(1/\lambda)}{dE}\right)_{ee}\frac{dl^{-1}(E')}{dE}\,l(E')\,dE'\,.\end{aligned} \tag{53}$$

In writing (51)–(53) we have made use of (50), (47), (44), and (42). In (53), $[d(1/\lambda)/dE]_{ee}$ is given by (31), while $[N_0(E)]_{SP}$ in (51) is the expression defined in (47). For $dl^{-1}(E')/dE$, we utilize the theoretical calculations of Ritchie and Ashley[45] (RA) for a degenerate free-electron gas. The work of RA yields

$$\left(\frac{dl^{-1}(E')}{dE}\right)_{RA} = \frac{\mu(E'-E)}{E'E_F}\,, \tag{54}$$

$$[l(E')]_{RA} = \frac{4E'E_F}{\mu(E'-E_F)^2}\,, \tag{55}$$

where μ is a constant depending on the density of the electron gas and a_0.

We have found that values of the MFP given by (55) are roughly a factor of 2 smaller than the experimental electron scattering lengths in Al compiled by Lindau and Spicer[44] for electron energies between ~5 and 10 eV above E_F. In our calculations for Al, we have accordingly used the following expression:

$$\frac{dl^{-1}(E')}{dE} = \frac{1}{2}\left(\frac{dl^{-1}(E')}{dE}\right)_{RA} = \frac{\mu(E'-E)}{2E'E_F}\,, \tag{56}$$

$$l(E') = 2[l(E')]_{RA} = \frac{8E'E_F}{\mu(E'-E_F)^2}\,. \tag{57}$$

Equations (57) and (56) describe quite well the rapid initial decrease of the experimental MFP[44] with increasing electron energy for $E' \lesssim 100$ eV. Around $E' \approx 100$ eV, the experimental MFP reaches a broad minimum and then increases with increasing energy.[43,44] Owing the assumptions made in its derivation,[45] the MFP given by (57) is a monotonically decreasing function of energy and fails completely to predict the observed behavior of the MFP's for $E' \gtrsim 100$ eV. Hence, (56) and (57) can only be used as approximate relations for $E' \lesssim 100$ eV in Al. In view of this observation, in our calculations for Al, we have set E_1, the upper limit in the scattering integral in the EDC from screened electron-electron interaction [Eq. (53)], equal to 100 eV, the approximate upper limit of validity for (56) and (57). For the EDC from volume-plasmon decay, we have set E_1 in the corresponding scattering integral [Eq. (52)] equal to 40 eV. Actually, for the EDC from volume-plasmon decay at least, the results do not depend very critically on the value of E_1 as long as $E_1 \gg E_F + \hbar\omega_p$. In fact, we have found that $[N(E)]_{VP}$ for Al calculated via (52) with $E_1 = 100$ eV differs from that calculated with $E_1 = 40$ eV by no more than ~1% with respect to overall magnitude for $E \lesssim 12$ eV in vacuum (the maximum value of emitted SE energies considered in this paper). In view of this, we have set $E_1 = 40$ eV (rather than 100 eV) for the volume-plasmon-decay EDC to economize on computation time. Since, as we shall see, the EDC from volume-plasmon decay represents by far the dominant contribution to the total theoretical EDC, the previous observation implies that the exact value of E_1 is not very crucial to our theoretical results for Al.

Having explained our choice of E_1, we turn next to discuss the other parameters entering in our calculations. As was mentioned at the end of Sec. II, the maximum volume-plasmon wave number q_1 is set equal to a constant value of 0.2 Å^{-1} in our calculations for Al. (The considerations involved in selecting q_1 were outlined in Sec. II.) Having chosen q_1, the maximum scattering angle θ_1 for volume plasmons in (42) and (19) is determined via the relation (15). For the surface plasmons, we have decided to set the maximum scattering angle θ_1 in (47) equal to $\theta_{ES} = \hbar\omega_s/2E_0$. For $E_0 = 1$ keV, this choice of θ_1 implies a maximum surface-plasmon wave number ~0.08 Å^{-1} (assuming $\hbar\omega_s = 10.6$ eV; see below). The corresponding minimum surface-plasmon wavelength is ~75 Å $\gg a$ (unit-cell dimension). Again, we expect that with this choice of minimum surface-plasmon wave-

length, the dipole approximation may still be reasonably valid. {The excitation probability for surface plasmons decreases very rapidly with increasing scattering angle, $\sim\theta^{-3}$ [cf. Eq. (34)] for large θ. Also, the EDC from surface-plasmon decay will be seen to constitute the smallest fraction of the total EDC in Al. A rigorous determination of θ_1 in (47) should therefore not be very critical.}

Concerning the choice of the broadening constants Γ_s and Γ_v in Al, the following remarks are in order. The existing experimentally determined long-wavelength limits of the surface- and volume-plasmon damping constants in Al quoted in the literature vary considerably from author to author depending on the technique used (optical measurements or electron-energy-loss spectroscopy).[46,47] Furthermore, both Γ_s and Γ_v are expected to depend strongly on the particular sample studied; in particular, Γ_s depends on the exact nature of the surface (crystallographic plane if single crystal). Hence, a unique choice of Γ_s and Γ_v for all cases is probably not feasible. In view of this, we have decided to treat Γ_s and Γ_v as adjustable parameters, allowing them to vary within reasonable limits. We have found that by setting $\Gamma_s = 1$ eV and $\Gamma_v = 2$ eV, very good agreement is obtained between our theoretical EDC's for Al and the experimental results that we shall consider later.[48]

For $\hbar\omega_p$, the volume-plasmon energy in Al, we use a value of 15 eV.[49] For $\hbar\omega_s$, the surface-plasmon energy, we use a value of 10.6 eV ($\hbar\omega_p/\sqrt{2}$). Finally, for the pseudopotential form factor, we use Ashcroft's[50] fit to Fermi-surface data, which gives for $|W_{111}|$ and $|W_{200}|$ the values 0.24 and 0.76 eV, respectively.

Having decided on the values of the various parameters mentioned above, the various EDC's given by (51)–(53) have been evaluated numerically for Al using $E_F = 11.6$ eV and $\Phi = 4.0$ eV for $E_0 = 1$ and 2 keV, respectively. The results are summarized in Figs. 4 and 5, which show the external SE EDC's and their derivatives (obtained by the spline-fit technique).

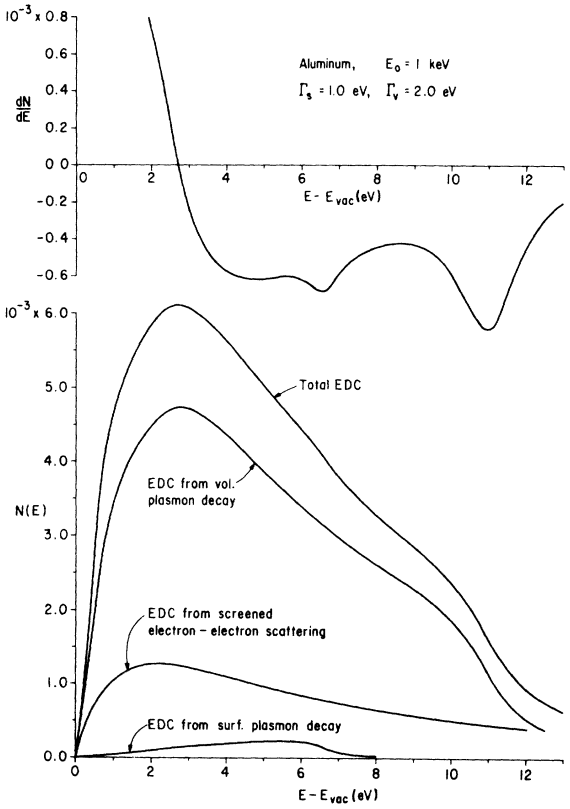

FIG. 4. Theoretical secondary-electron energy distribution curve $N(E)$ and its derivative dN/dE for aluminum plotted versus secondary-electron energy in vacuum ($E - E_{vac}$) for $E_0 = 1$ keV (primary energy). The contributions to $N(E)$ from volume-plasmon decay, screened electron-electron scattering and surface-plasmon decay are also shown separately. For the results shown here, Γ_s and Γ_v have been given the values 1.0 and 2.0 eV, respectively.

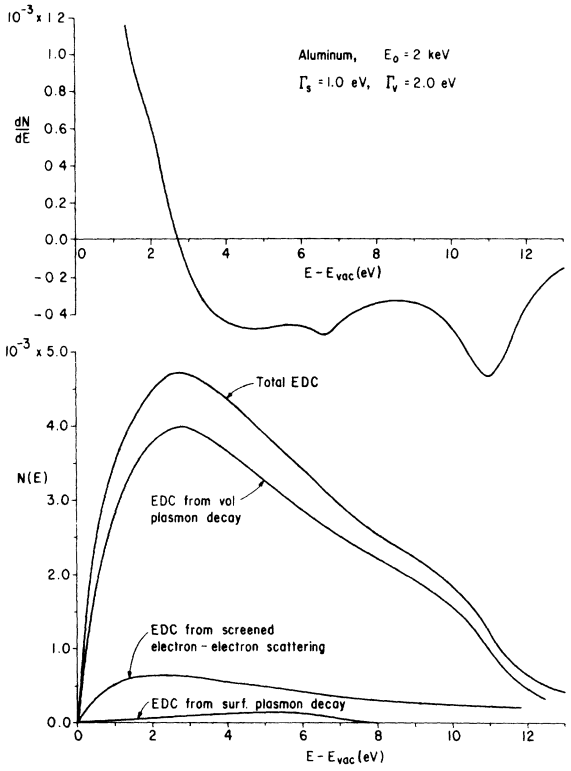

FIG. 5. Same quantities for aluminum as in Fig. 6 but with $E_0 = 2$ keV. Γ_s and Γ_v have the same values as in Fig. 6.

The most significant feature of our results is the existence of two prominent humps in the EDC's that are clearly discerned as minima in the derivatives of the EDC's. These minima occur at SE kinetic energies in vacuum equal approximately to 6.6 and 11.0 eV, corresponding to $\hbar\omega_s - \Phi$ and $\hbar\omega_p - \Phi$ in Al. From Figs. 4 and 5, which show the various contributions to the total EDC, we see that the two humps are due to the EDC's provided by surface- and volume-plasmon decay, respectively.

To test the validity of our theoretical results for the SE EDC in Al, we compare them with the available experimental data. We have for instance the published results obtained by Jenkins and Chung,[23] Powell and Woodruff,[25] Henrich,[24] and the very recent data obtained by Cailler *et al.*[51] and by Everhart *et al.*[26] All of these experimental results were obtained from clean Al samples in ultrahigh-vacuum conditions. We shall select the data obtained by the last-mentioned authors[26] for detailed comparison with our theoretical results. These authors performed their measurements on a polycrystalline Al sample (in ultrahigh vacuum) whose surface was cleaned by argon-ion bombardment and monitored by Auger-electron spectroscopy. The details of the experiment can be found in Ref. 26. Figure 6 shows some of their experimental results.

By comparing the experimental curves in Fig. 6 with our theoretical EDC's and their derivatives, we see that there exists good overall agreement between theory and experiment. In particular, the two pieces of structure appearing in the theoretical results are confirmed by the experimental data with respect to both overall shapes and approximate energy locations. We should not expect exact quantitative agreement because of the many simplifying assumptions used in our theoretical developments. We remark that had we neglected the once-scattered electrons in the EDC from volume-plasmon decay in Al, the agreement achieved between theory and experiment concerning the total EDC would be severely diminished.

We have also compared our theoretical EDC's with experimental data reported in Refs. 23–25 and 51. In all cases, good qualitative agreement between theory and experiment is obtained with respect to the presence of the two humps in the EDC and its overall shape. By numerically integrating our theoretical EDC's from $E = 0$ to 50 eV, we have calculated the number of so-called "true" SE's, denoted by δ_0, which are produced by the incident primary electron alone. (True SE's are also created by backscattered primary electrons. For a good discussion, see Ref. 52.) We have compared our theoretical δ_0 for Al with

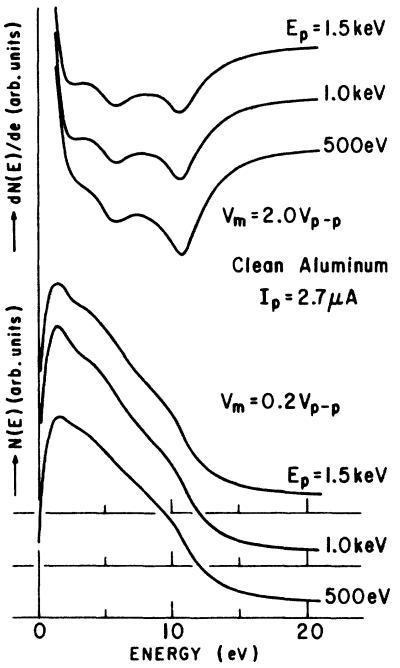

FIG. 6. Experimental results for aluminum obtained by Everhart *et al.* (after Ref. 26). Shown are the secondary-electron energy distribution curve $N(E)$ and its derivative dN/dE as a function of secondary-electron kinetic energy in vacuum ($E - E_{vac}$). E_p is the incident primary energy, I_p is the incident-beam current, while V_m is the modulating voltage used to obtain $N(E)$ and dN/dE.

the experimentally determined values reported by Bronshtein and Fraiman[53] for two different values of primary energy. The theoretical and experimental values of δ_0 are listed in Table I. Our theoretical values are too low by roughly a factor of 3.

VII. SUMMARY AND DISCUSSION

In this paper, we have carried out a theoretical analysis of SEE in the NFE metals, restricting ourselves to excitations from the valence band. We have found that in the case of Al, the decay of long-wavelength surface and volume plasmons excited by the incident primary are important

TABLE I. Comparison of theoretical and experimental values of the secondary-electron yield δ_0 produced by the incident primary electrons alone.

Theory		Experiment (Ref. 53)	
Primary energy, E_0 (keV)	δ_0	Primary energy, E_0 (keV)	δ_0
1.0	0.051	1.2	0.15
2.0	0.038	2.0	0.13

mechanisms of SE generation. Our theoretical EDC's are in good agreement with recent experimental results. Such would not be the case if we had neglected the contributions from the plasmons. The theoretical SE yield δ_0 is about a factor of 3 smaller than experimental values. This discrepancy suggests that our choice of q_1, the maximum volume-plasmon wave number [or equivalently, $\lambda_{eff}^{-1}(E_0, \theta_1)$], may be too conservative. Haque and Kliewer[54] have studied the volume-plasmon properties in Na and K. The Bloch electron RPA scheme was used in conjunction with an augmented-plane-wave approach. For q along the [110] and [100] directions, it was found that plasmon damping is almost entirely caused by interband transitions even for q values comparable to q_c, the critical value for the onset of Landau damping. Analogous calculations do not as yet exist for Al. However, if we extrapolate the results for Na and K to Al and allow the maximum volume-plasmon wave number in our calculations to equal $\sim q_c$, we find that the discrepancy between theory and experiment with respect to δ_0 is to a large degree eliminated. Such an extrapolation may not be unreasonable, since Na and K are even more nearly-free-electron-like than Al in terms of their band structures.

The question may be raised that the most significant physical process emplasized here, namely, low-q plasmon decay may be uniquely important for aluminum only. In this connection, Höhberger *et al.*,[55-57] based on their experimental investigation of the small-q volume-plasmon dispersion relation, have suggested that parallel band transitions give aluminum unique low-q plasmon characteristics. However, as we have pointed out in the footnote under Ref. 34, the contributions to $\epsilon_2(q \approx 0, \omega)$ from parallel band transitions terminate at frequencies significantly below ω_p in Al. As was pointed out in Ref. 46, only normal, Butcher-type transitions should be important in causing low-q plasmon decay [determined by $\epsilon_2(q \approx 0, \omega_p)$] in Al and other NFE metals. Hence, we believe that the conclusion reached here, that low-q plasmon decay plays an important role in SEE, is not restricted to Al alone but should be valid in other NFE metals as well. In this connection, we should like to point out that we have also carried out analogous calculations of the SE EDC in Mg using the formalism described in this paper.[58] The resulting EDC's are in quite good agreement with some recent experimental EDC's obtained from clean Mg surfaces under ultrahigh-vacuum conditions.[59] In particular, humps similar to those in Al are found in the theoretical EDC at $\hbar\omega_p - \Phi$ and $\hbar\omega_s - \Phi$, and are confirmed by the experimental data.

In our theory, we have made a number of simplifying approximations, e.g., the Thomas-Fermi approximation in Sec. III and our highly idealized SE transport model. However, the satisfactory agreement obtained between theory and experiment regarding the SE EDC in Al suggests that the theory that we have outlined provides a reasonably correct physical picture of SEE in the NFE metals. In conclusion, while much more work remains to be done before overall quantitative agreement between theory and experiment can be achieved, we believe that the present paper represents the first theoretical demonstration of the importance of volume- and surface-plasmon decay in SEE from clean surfaces of NFE metals.

ACKNOWLEDGMENTS

We are grateful to Professor L. M. Falicov of the Physics Department for a number of very stimulating and helpful discussions concerning various aspects covered in this paper and for a critical reading of the manuscript. In addition we would like to thank Professor R. Shimizu and his colleagues at Osaka University for their collaboration in obtaining the experimental results on aluminum discussed in this paper and for many fruitful discussions. One of us (M.S.C.) wishes to express his gratitude to the Joint Services Electronics Program for a Research Assistantship and the other (T.E.E.) is grateful to the John Simon Guggenheim Memorial Foundation for financial support during the period when much of the work reported here was done.

APPENDIX A

In this appendix, we give a concise derivation of Eq. (1) in the text. The transition rate for an incident fast electron to transfer momentum $\hbar\vec{q} = \hbar(\vec{K}_0 - \vec{K}_1)$ and energy $\hbar\omega = E_0 - E_1$ to the solid is given by the standard expression[14,15]

$$W(\vec{q}, \omega) = \frac{-8\pi e^2}{\Delta \hbar q^2} \operatorname{Im}\left(\frac{1}{\epsilon(\vec{q}, \omega)}\right). \tag{A1}$$

In (A1), $\epsilon(\vec{q}, \omega)$ is the longitudinal dielectric constant. Writing $\operatorname{Im}[1/\epsilon(\vec{q}, \omega)]$ as $-\epsilon_2(\vec{q}, \omega)/|\epsilon(\vec{q}, \omega)|^2$, where $\epsilon(\vec{q}, \omega) = \epsilon_1(\vec{q}, \omega) + i\epsilon_2(\vec{q}, \omega)$, we have

$$W(\vec{q}, \omega) = \frac{8\pi e^2}{\Delta \hbar q^2} \frac{\epsilon_2(\vec{q}, \omega)}{|\epsilon(\vec{q}, \omega)|^2}. \tag{A2}$$

Using the RPA for Bloch electrons, we can write,[14,27] neglecting local field and umklapp effects,

$$[\epsilon_2(\vec{q},\omega)]_{\mathrm{RPA}}=\frac{4\pi^2e^2}{\Delta q^2}\sum_{l'l,\vec{k}'\vec{k}}|(l'\vec{k}'|l\vec{k})|^2\times\delta_{\vec{k}',\vec{k}+\vec{q}}\,\delta(\hbar\omega-E_{l'\vec{k}'}+E_{l\vec{k}}). \tag{A3}$$

In (A3), all the terms and symbols have been explained in the text. Substituting (A3) into (A2), we have

$$W(\vec{q},\omega)=\frac{32\pi^3e^4}{\hbar\Delta^2q^4}\sum_{l'l,\vec{k}'\vec{k}}\frac{|(l'\vec{k}'|l\vec{k})|^2}{|\epsilon(\vec{q},\omega)|^2}\times\delta_{\vec{k}',\vec{k}+\vec{q}}\delta(\hbar\omega-E_{l'\vec{k}'}+E_{l\vec{k}}). \tag{A4}$$

In (A4), it is understood that the Bloch-electron RPA form for $\epsilon(\vec{q},\omega)$ is used. From (A4) it is apparent that the transition rate for the process in which the Bloch state $|l\vec{k}\rangle$ is excited into the final state $|l'\vec{k}'\rangle$ with momentum and energy transfer $(\vec{q},\omega)$ is given by

$$W(l\vec{k}\to l'\vec{k}')=[W(\vec{q},\omega)]_{l\vec{k}-l'\vec{k}'}=\frac{32\pi^3e^4}{\hbar\Delta^2q^4}\frac{|(l'\vec{k}'|l\vec{k})|^2}{|\epsilon(\vec{q},\omega)|^2}\times\delta_{\vec{k}',\vec{k}+\vec{q}}\delta(\hbar\omega-E_{l'\vec{k}'}+E_{l\vec{k}}). \tag{A5}$$

Equation (A5) is precisely Eq. (1) in the text. We note of course that $|l\vec{k}\rangle$ must be initially occupied and $|l'\vec{k}'\rangle$ unoccupied.

APPENDIX B

In this appendix, we give an outline of the evaluation of Eq. (27) in the text. We want to calculate

$$W_T(\vec{k}')=\sum_{\vec{q}}\frac{32\pi^3e^4f_0(E_{\vec{k}-\vec{q}})[1-f_0(E_{\vec{k}'})]\delta(E_{\vec{k}'}-E_{\vec{k}'-\vec{q}}-\hbar\omega)}{\Delta^2\hbar(q^2+q_{\mathrm{FT}}^2)^2}. \tag{B1}$$

We remember that

$$\hbar\omega=\frac{\hbar^2K_0^2}{2m}-\frac{\hbar^2}{2m}(\vec{K}_0-\vec{q})^2, \tag{B2}$$

where $\vec{K}_0$ is the wave vector of the incident primary electron. The summation over $\vec{q}$ in (B1) is equivalent to summing over all initial states lying inside the Fermi sphere. Consider Fig. 7; $\vec{k}'$ is the final wave vector of the excited crystal electron while $\vec{k}'-\vec{q}$ is the initial wave vector. The Fermi sphere is shown with radius k_F. We must obviously have $k'>k_F$ and $|\vec{k}'-\vec{q}|\le k_F$.

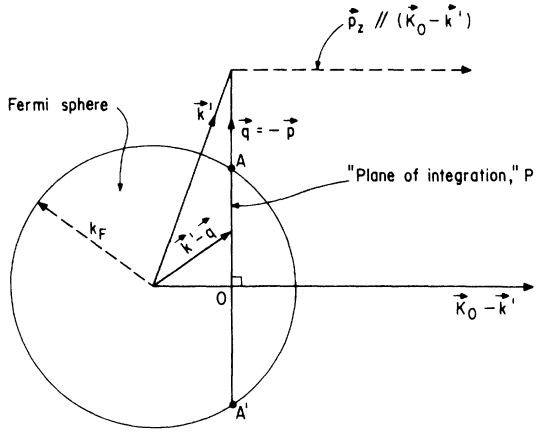

FIG. 7. Diagram in wave-vector space illustrating the evaluation of Eq. (27) in the text.

Now the δ function in (B1) can be written as

$$\delta(E_{\vec{k}'}-E_{\vec{k}'-\vec{q}}-\hbar\omega)=\delta\left(\frac{\hbar^2k'^2}{2m}-\frac{\hbar^2(\vec{k}'-\vec{q})^2}{2m}-\frac{\hbar^2K_0^2}{2m}+\frac{\hbar^2}{2m}(\vec{K}_0-\vec{q})^2\right)=\frac{m}{\hbar^2}\delta(\vec{q}\cdot(\vec{K}_0-\vec{k}')). \tag{B3}$$

Substituting (B3) into (B1) and dropping the f_0's,

$$W_T(\vec{k}')=\sum_{\vec{q}}\frac{32\pi^3e^4m\,\delta(\vec{q}\cdot(\vec{K}_0-\vec{k}'))}{\Delta^2\hbar^3(q^2+q_{\mathrm{FT}}^2)^2} \tag{B4}$$

$$=\int\frac{4me^4\delta(\vec{q}\cdot(\vec{K}_0-\vec{k}'))\,d\vec{q}}{\Delta\hbar^3(q^2+q_{\mathrm{FT}}^2)^2}. \tag{B5}$$

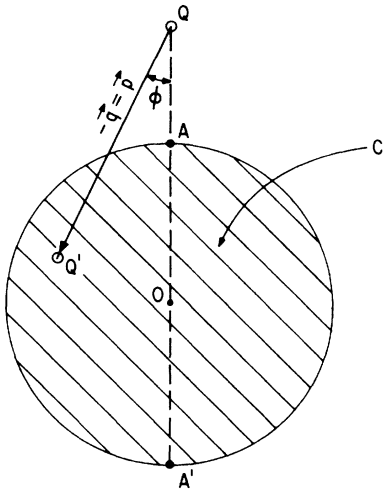

FIG. 8. End view (along $\vec{K}_0-\vec{k}'$) of the circular disk C, which is denoted by AOA' in Fig. 7. Q and Q' are the end points of $\vec{k}'$ and $\vec{k}'-\vec{q}$, respectively. Q' (for fixed Q) must lie inside or on the circumference of C; i.e., it must lie inside the shaded region in the figure.

In (B5), we integrate over all momentum transfers $\vec{q}$ such that $|\vec{k}'-\vec{q}|\le k_F$. Letting $\vec{p}=-\vec{q}$ (see Fig. 7), (B5) can be rewritten as

$$W_T(\vec{k}')=\frac{4me^4}{\Delta\hbar^3}\int\frac{\delta(\vec{p}\cdot(\vec{K}_0-\vec{k}'))\,d\vec{p}}{(p^2+q_{FT}^2)^2}. \tag{B6}$$

Letting the p_z axis be parallel to $\vec{K}_0-\vec{k}'$ and passing through the end point to $\vec{k}'$, denoting the polar and azimuthal angles of $\vec{p}$ by θ and ϕ,

$$W_T(\vec{k}')=\frac{4me^4}{\Delta\hbar^3|\vec{K}_0-\vec{k}'|}\iiint_{|\vec{k}'+\vec{p}|\le k_F}\frac{p\delta(\cos\theta)\,dp\,d(\cos\theta)\,d\phi}{(p^2+q_{FT}^2)^2} \tag{B7}$$

$$=\frac{4me^4}{\Delta\hbar^3|\vec{K}_0-\vec{k}'|}\iint_{|\vec{k}'+\vec{p}|\le k_F}\frac{p\,dp\,d\phi}{(p^2+q_{FT}^2)^2}. \tag{B8}$$

In (B8), the integrations are to be carried out for $\vec{p}$ lying on a plane perpendicular to $\vec{K}_0-\vec{k}'$ and passing through the end point of $\vec{k}'$. This plane is denoted by P in Fig. 7. In addition, we must have $|\vec{k}'+\vec{p}|\le k_F$. These two restrictions imply that the allowable $\vec{p}$ vectors and initial states $\vec{k}'+\vec{p}$ are restricted to have their end points lying within or on the circumference of the circular disk formed by the intersection of the plane P with the Fermi sphere. This circular disk is shown in Fig. 8, which shows the geometry as viewed along $\vec{K}_0-\vec{k}'$. The integrals in (B8) are then restricted within the area of this circular disk, denoted by C in Fig. 8. Hence,

$$W_T(\vec{k}')=\frac{4me^4}{\Delta\hbar^3|\vec{K}_0-\vec{k}'|}\iint_C\frac{p\,dp\,d\phi}{(p^2+q_{FT}^2)^2}. \tag{B9}$$

Equation (B9) can be evaluated exactly. The exact details are straightforward but extremely tedious. We shall not reproduce them here. Rather, we shall just state the final result:

$$W_T(\vec{k})=\frac{2\pi me^4}{\Delta\hbar\,|\vec{K}_0-\vec{k}'|\,q_{FT}^2}\left\{1-(k'^2-k_F^2+q_{FT}^2)\left[(k'^2-k_F^2)^2+2q_{FT}^2\left(k'^2+k_F^2-\frac{2|\vec{k}'\cdot(\vec{K}_0-\vec{k}')|^2}{|\vec{K}_0-\vec{k}'|^2}\right)+q_{FT}^4\right]^{-1/2}\right\} \tag{B10}$$

for $|\vec{k}'\cdot(\vec{K}_0-\vec{k}')|\le k_F|\vec{K}_0-\vec{k}'|$; and $W_T(\vec{k}')=0$, otherwise.

The condition on $|\vec{k}'\cdot(\vec{K}_0-\vec{k}')|$ simply reflects the fact that when $|\vec{k}'\cdot(\vec{K}_0-\vec{k}')|>k_F|\vec{K}_0-\vec{k}'|$, the "plane of integration" P does not intersect the Fermi sphere and so no allowable initial state can give rise to the final state $\vec{k}'$.

Finally, (B10) with $\vec{k}'$ relabeled by $\vec{k}$ gives (28) in the text.

*Research sponsored by the Joint Services Electronics Program under Contract F44620-76-C-0100.

[1]A. J. Dekker and A. van der Ziel, Phys. Rev. 86, 755 (1952).
[2]A. van der Ziel, Phys. Rev. 92, 35 (1953).
[3]P. A. Wolff, Phys. Rev. 95, 56 (1954).
[4]H. W. Streitwolf, Ann. Phys. (Leipz.) 3, 183 (1959).
[5]H. Stolz, Ann. Phys. (Leipz.) 3, 197 (1959).
[6]A. I. Guba, Sov. Phys.-Solid State 4, 1197 (1962).
[7]A. I. Grinchak, Sov. Phys.-Solid State 8, 1000 (1966).
[8]G. F. Amelio, J. Vac. Sci. Technol. 7, 593 (1970).
[9]T. E. Everhart and M. S. Chung, J. Appl. Phys. 43, 3707 (1972).
[10]M. S. Chung and T. E. Everhart, J. Appl. Phys. 45, 707 (1974).
[11]M. S. Chung, J. Appl. Phys. 46, 465 (1975).
[12]A. J. Dekker, Solid State Phys. 6, 251 (1958).
[13]O. Hachenberg and W. Brauer, Adv. Electron. Electron Phys. 11, 413 (1959).
[14]D. Pines, *Elementary Excitations in Solids* (Benjamin, New York, 1964).
[15]P. Nozières and D. Pines, *Theory of Quantum Liquids*, (Benjamin, New York, 1966).
[16]H. Raether, Springer Tracts Mod. Phys. 38, 84 (1965).
[17]K. D. Sevier, in *Low Energy Electron Spectrometry* (Interscience, New York, 1972), Chap. 8.
[18]D. Pines, Physica (Utr.) 26, S103 (1960).
[19]R. A. Ferrell, Phys. Rev. 111, 1214 (1958).
[20]W. Steinmann and M. Skibowski, Phys. Rev. Lett. 16, 989 (1966).
[21]N. B. Gornyi, Sov. Phys.-Solid State 8, 1535 (1966).
[22]N. B. Gornyi, L. M. Rakhovich, and S. F. Skirko, Sov. Phys. J. 10, 15 (1967).
[23]L. H. Jenkins and M. F. Chung, Surf. Sci. 28, 409 (1971).
[24]V. E. Henrich, Phys. Rev. B 7, 3512 (1973).
[25]B. D. Powell and D. P. Woodruff, Surf. Sci. 33, 437 (1972).
[26]T. E. Everhart, N. Saeki, R. Shimizu, and T. Koshikawa, J. Appl. Phys. 47, 2941 (1976).
[27]H. Ehrenreich and M. H. Cohen, Phys. Rev. 115, 786 (1959).
[28]R. H. Ritchie, Phys. Rev. 114, 644 (1959).
[29]H. Ehrenreich, in *Optical Properties of Sdids*, edited by J. Tauc (Academic, New York, 1966), p. 106.
[30]R. Y. Koyama and N. V. Smith, Phys. Rev. B 2, 3049 (1970).
[31]W. A. Harrison, *Pseudopotentials in the Theory of Metals* (Benjamin, New York, 1966).
[32]N. W. Ashcroft and K. Sturm, Phys. Rev. B 3, 1898 (1971).
[33]N. V. Smith and W. E. Spicer, Phys. Rev. 188, 593

(1969).

[34]In polyvalent NFE metals like Al, another important contribution to optical absorption is the so-called parallel band absorption involving transitions between near-parallel bands near the Brillouin-zone faces. However, as Ashcroft and Sturm (Ref. 32) have pointed out, the contribution of this type of transitions to the real part of the conductivity (or imaginary part of the dielectric constant) terminates at a definite frequency ω_0 depending on the particular reciprocal-lattice vector involved. For instance, for the case of Al, using Eq. (A3) of Ref. 32, parallel band absorption ceases at an energy equal to 8 eV for $\vec{G}_{111}$ and 4 eV for $\vec{G}_{200}$. These energies are much lower than $\hbar\omega_p$, the volume-plasmon energy in Al. Hence, for the purpose of describing volume-plasmon decay, this type of transition should not be important. Only normal interband transitions (which form the continuation to the conductivity beyond ω_0) need be considered. This conclusion is expected to be valid for other NFE metals, particularly the monovalent alkalis, where parallel band transitions (similar to those in Al) do not occur. [In this connection, see also the discussion by A. G. Mathewson and H. P. Myers, J. Phys. F 3, 623 (1973).]

[35]We wish to thank Professor L. M. Falicov for a discussion concerning the validity of the dipole approximation and the criteria stated here.

[36]We give here some justifications for the results obtained in Sec. III. Virtually all previous significant theoretical work in SEE have used an excitation function derived by Streitwolf (Ref. 4) employing an *unscreened* Coulomb potential to treat the primary-electron–valence-electron scattering. (See, for instance, Refs. 5–8 and 42.) Owing to the long range of the unscreened Coulomb potential, the expression derived by Streitwolf diverges for $E \to E_F$, where E is the excited SE energy. {In our notation, the expressions derived by Streitwolf corresponding to our Eq. (31) is given by $[d(1/\lambda)/dE]_S = e^4 k_F^3/3\pi E_0(E-E_F)^2$, demonstrating the singularity at $E=E_F$.} Nevertheless, Streitwolf's result is expected to be reasonably accurate for $E-E_F >> E_F$, a regime in which screening is unimportant since the momentum transfers involved are large. The unphysical divergence in $[d(1/\lambda/dE]_S$ at small values of $E-E_F$ is removed by our result, Eq. (31), which considers dielectric screening (although in an approximate way only). It can be shown that our Eq. (31) reduces to Streitwolf's expression in the limit $q_{TF} \to 0$ (no screening), as it should. In addition, our Eq. (31) approaches Streitwolf's result asymptotically for $E-E_F >> E_F$, the energy region in which the latter is expected to be reasonably accurate. (This is not surprising as the Thomas-Fermi dielectric constant approaches unity for q very large.) Our Eq. (31) represents therefore an improvement over Streitwolf's unscreened result, which has been used almost exclusively by previous authors. Hence there is some merit in using the results obtained in Sec. III even though they are not completely justifiable for all values of SE energies considered.

[37]R. H. Ritchie, Phys. Rev. 106, 874 (1957).

[38]Modifications brought about by retardation effects in the surface-plasmon (SP) properties are only important for values of Q (SP wave number) such that $Q \lesssim \omega_p/c$ ($\sim 8\times 10^{-3}$ Å^{-1} in Al). However, as Economou [Phys. Rev. 182, 539 (1969)] and Ngai *et al.* [Phys. Rev. Lett. 24, 61 (1970)] have pointed out, the SP fields tend to zero in the region of Q space where retardation is important. Hence, the coupling of the SP fields to incident fast electrons will be negligible precisely for this region of q space. In a first-order calculation of the SP excitation probability by incident electrons, retardation effects can thus be disregarded.

[39]E. A. Stern and R. A. Ferrell, Phys. Rev. 120, 130 (1960).

[40]J. G. Endriz and W. E. Spicer, Phys. Rev. B 4, 4159 (1971).

[41]C. N. Berglund and W. E. Spicer, Phys. Rev. 136, A1030 (1964).

[42]A. J. Bennett and L. M. Roth, Phys. Rev. B 5, 4309 (1972).

[43]P. W. Palmberg, Anal. Chem. 45:6, 549A (1973).

[44]I. Lindau and W. E. Spicer, J. Electron Spectrosc. 3, 409 (1974).

[45]R. H. Ritchie and J. C. Ashley, J. Phys. Chem. Solids 26, 1689 (1965).

[46]For instance, Elson and Ritchie [Surf. Sci. 30, 178 (1972)], from analysis of optical data on Al, quote a value of 0.57 eV for Γ_s, the surface-plasmon damping constant. Bagchi *et al.* [Phys. Rev. Lett. 27, 998 (1971)], from analysis of inelastic low-energy-electron-diffraction data, quote a value of 0.9 eV for the same quantity. Duke and Landman [Phys. Rev. B 8, 505 (1973)], using the same method as Bagchi *et al.*, give a value of 1.85 eV for Γ_s.

[47]For the $q \approx 0$ volume-plasmon damping constant in Al, Γ_v, values given in the literature range generally from 0.5 to 1.0 eV depending on the experimental method used (optical measurements or electron-energy-loss spectroscopy) and sample studied. See the table appearing in Ref. 49.

[48]The value of Γ_s used is within the range of the experimental values while Γ_v is somewhat higher than the experimental numbers. We must not forget that we are considering plasmons with a finite wave number and that Γ_v increases with q.

[49]J. Geiger and K. Wittmaack, Z. Phys. 195, 44 (1966).

[50]N. W. Ashcroft, Philos. Mag. 8, 2055 (1963).

[51]M. Cailler (private communication). Also reported as an experimental result by J. P. Ganachaud and M. Cailler, in Second Colloque Internationale de Physique et Chemie des Surfaces, Université de Bretagne Occidentale, Brest, 1975 (unpublished).

[52]H. Seiler, Z. Angew. Phys. 22:3, 249 (1967).

[53]I. M. Bronshtein and B. S. Fraiman, Sov. Phys.-Solid State 3, 1188 (1961).

[54]M. S. Haque and K. L. Kliewer, Phys. Rev. B 7, 2416 (1973).

[55]H. J. Höhberger, A. Otto, and E. Petri, Fourth International Conference on VUV, 1974 Extended Abstract 68 and 69 (unpublished).

[56]H. J. Höhberger, A. Otto, and E. Petri, Solid State Commun. 16, 175 (1975); E. Petri and A. Otto, Phys. Rev. Lett. 34, 1283 (1975).

[57]We are grateful to Dr. Kenneth L. Kliewer for bringing Refs. 55 and 56 to our attention.

[58]M. S. Chung, Ph.D. thesis, (University of California, Berkeley, 1976) (unpublished).

[59]L. H. Jenkins and M. F. Chung, Surf. Sci. 33, 159 (1972); B. Wright and E. B. Pattinson, J. Phys. F 3, 1237 (1973); 4, 176 (1974).